Journal of
Materials Chemistry C

Accepted Manuscript

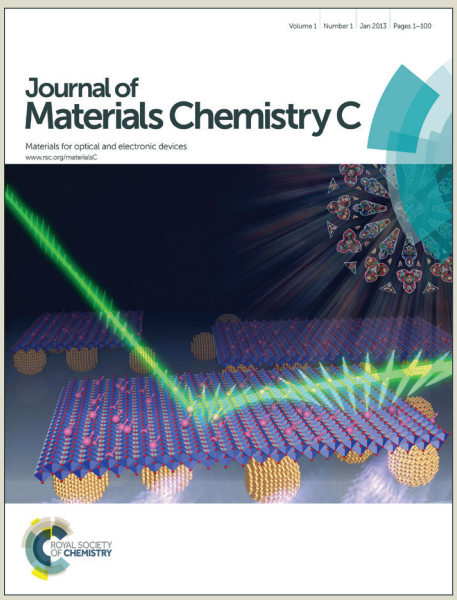

This is an *Accepted Manuscript*, which has been through the Royal Society of Chemistry peer review process and has been accepted for publication.

Accepted Manuscripts are published online shortly after acceptance, before technical editing, formatting and proof reading. Using this free service, authors can make their results available to the community, in citable form, before we publish the edited article. We will replace this *Accepted Manuscript* with the edited and formatted *Advance Article* as soon as it is available.

You can find more information about *Accepted Manuscripts* in the Information for Authors.

Please note that technical editing may introduce minor changes to the text and/or graphics, which may alter content. The journal's standard Terms & Conditions and the Ethical guidelines still apply. In no event shall the Royal Society of Chemistry be held responsible for any errors or omissions in this *Accepted Manuscript* or any consequences arising from the use of any information it contains.

ROYAL SOCIETY OF CHEMISTRY

www.rsc.org/materialsC

Synthesis, Crystal Structure, and Thermoelectric Properties of Two New Barium Antimony Selenides: $Ba_2Sb_2Se_5$ and $Ba_6Sb_7Se_{16.11}$

Jian Wang, Kathleen Lee, Kirill Kovnir*

Department of Chemistry, University of California, Davis,

One Shields Avenue, Davis, CA 95616, United States

Journal of Materials Chemistry C Accepted Manuscript

TOC Entry

Two new antimony selenides crystallizing in new structure types, $Ba_2Sb_2Se_5$ and $Ba_6Sb_7Se_{16.11}$, were synthesized and characterized. The structural complexity and disorder in the Se sublattice of $Ba_2Sb_2Se_5$ resulted in extremely low thermal conductivity.

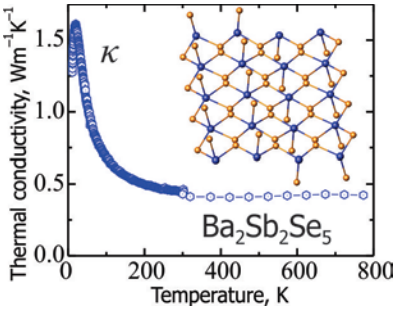

Journal of Materials Chemistry C Accepted Manuscript

Abstract

Two new antimony selenides, $Ba_2Sb_2Se_5$ and $Ba_6Sb_7Se_{16.11}$, were synthesized via high-temperature solid-state reactions and their structures were determined by single crystal X-ray diffraction. Both of the title compounds crystallize in two new structure types in orthorhombic space groups, $Ba_2Sb_2Se_5$: *Pbam* (No. 55) $Z = 4$, $a = 8.403(2)$ Å; $b = 27.567(5)$ Å; $c = 4.6422(8)$ Å; and $Ba_6Sb_7Se_{16}$: *Pnnm* (No. 58) $Z = 4$, $a = 12.469(2)$ Å; $b = 62.421(7)$ Å; $c = 4.6305(5)$ Å. The crystal structures of both phases contain Sb-Se slabs and one-dimensional Ba-Se chains that are not commonly found in alkaline-earth antimony selenides. $Ba_2Sb_2Se_5$ is an *n*-type semiconductor with a bandgap close to 1 eV as revealed by resistivity measurements and UV-visible spectroscopy. Due to the complex crystal structure and disorder in the Se sublattice, $Ba_2Sb_2Se_5$ exhibits extremely low thermal conductivity (0.4 $Wm^{-1}K^{-1}$) from room temperature to 800 K.

Journal of Materials Chemistry C Accepted Manuscript

Introduction:

Ternary and quaternary antimony chalcogenides exhibit rich structural chemistry, which results in a large variety of physical properties. Various SbQ_n (Q = S, Se; n = 3, 4, 5) units are present in the crystal structures of these compounds as either isolated fragments or as parts of extended finite and infinite chains, slabs, layers, and frameworks. The presence of the Sb^{3+} stereoactive $5s^2$ electron lone pair adds to the structural diversity of these compounds. Antimony selendides are considered promising materials for non-linear optics,[1-2], thermoelectrics,[3-11] and magnetic applications.[12,13] The structural complexity of low-dimensional antimony chalcogenides may result in promising thermoelectric properties, such as low lattice thermal conductivity. Inspired by the structural complexity we explored the Ba-Sb-Se system.

Prior to our work, only two compounds were structurally characterized in the Ba-Sb-Se system: $Ba_4Sb_4Se_{11}$ [14] and $BaSb_2Se_4$.[15] We have recently reported another compound, $Ba_3Sb_2Se_7$, containing isolated $SbSe_3$ and $SbSe_4$ fragments in the crystal structure.[16] Herein we describe two new compounds, $Ba_2Sb_2Se_5$ and $Ba_6Sb_7Se_{16.11}$, which crystallize in new structure types. In their crystal structures, one- ($Ba_2Sb_2Se_5$) and two-dimensional ($Ba_6Sb_7Se_{16.11}$) Sb-Se fragments alternate with one-dimensional Ba-Se bands and additional Ba atoms. Detailed characterization of the optical, electrical, and thermal transport properties of $Ba_2Sb_2Se_5$ is also reported.

Journal of Materials Chemistry C Accepted Manuscript

Results and Discussion

Crystal structure. $Ba_2Sb_2Se_5$ and $Ba_6Sb_7Se_{16.11}$ were synthesized from elements via conventional high-temperature solid-state reactions and their crystal structures were determined using single crystal X-ray diffraction (Table 1). A common feature in the crystal structures of $Ba_2Sb_2Se_5$ and $Ba_6Sb_7Se_{16.11}$ is disorder in the Se sublattice (Table 2). Several Se positions in both structures are split into two positions with 50% occupancies (Figure 1). An unsplit "ideal" Se position would be coordinated by four Sb atoms forming a distorted square with relatively large Se-Sb distances of ~3 Å. The splitting of the Se positions leads to the formation of two Se positions with 50% occupancies. Each of the split Se atoms is two-coordinated by two Sb atoms on one side with significantly shorter Sb-Se distances (Figure 1). The occupancies of each pair of split positions were refined. Since the refined values did not deviate from 50% within one estimated standard deviation, the occupancies of the split positions were fixed to 50% in the final refinement (Table 2).

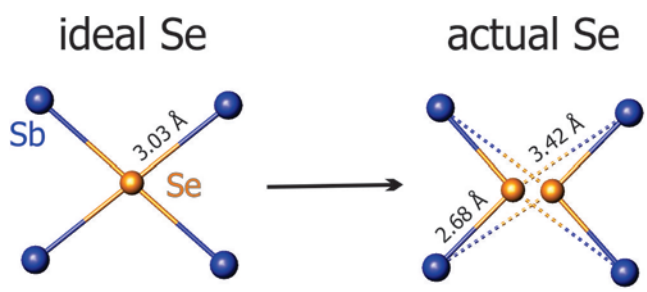

Figure 1. An example of the splitting of the ideal Se position inside an Sb_4 square into two partially occupied Se positions. Only one Se site is occupied, while the other is vacant. Each of the occupied Se positions is two-coordinated. Sb: blue; Se: orange.

The splitting of the Se positions leads to the alteration of the Sb coordination as shown in Figure 2 using the example of the ${}_{\infty}^{1}(Sb_4Se_9)^{6-}$ fragment that is present in the crystal structure of $Ba_2Sb_2Se_5$. In an ideal, unsplit situation, all Sb atoms are coordinated by five Se atoms forming a square pyramid (Figure 2, left). Splitting of the Se position results in the formation of two short bonds instead of four as shown in Figure 1. All possible Se positions are shown in the middle of Figure 2. Since the occupancies of all split Se positions is 50% the real coordination number of antimony is reduced to an average coordination of three Se atoms. Since no additional ordering

Journal of Materials Chemistry C Accepted Manuscript

of Se atoms was observed, the local coordination of Sb atoms with Se atoms may vary from one to five. While the coordination numbers of one and five are extremes with low probabilities of occurring, local Sb coordination numbers of two, three, and four Se atoms are more probable. A random model of the real coordination is shown in Figure 2, right. We believe that such local disorder has a dramatic impact on the thermal conductivity of this compound (*vide infra*). In Figure 3 all Se split sites are shown for $Ba_2Sb_2Se_5$ and $Ba_6Sb_7Se_{16.11}$.

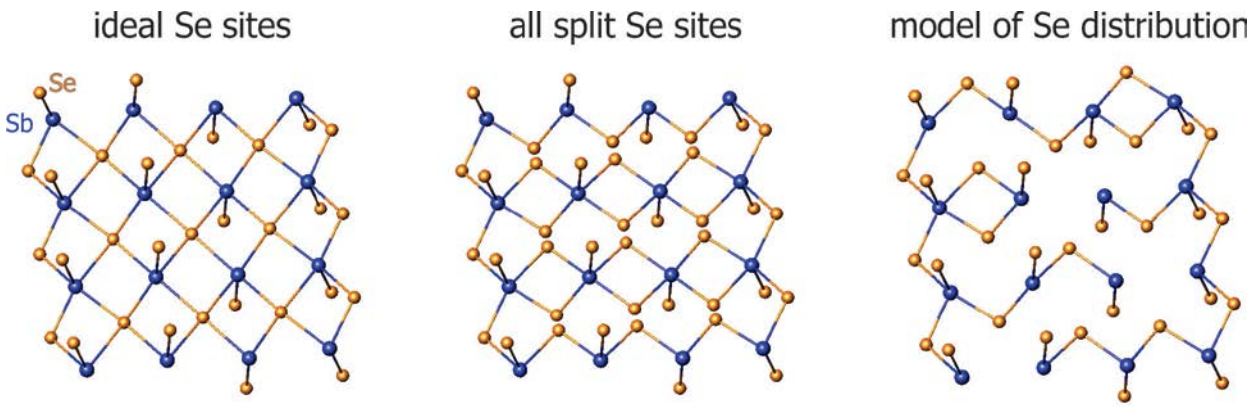

Figure 2. An example of the splitting of the ideal Se position inside a Sb_4 square into two Se split positions in the ${}_{\infty}^{1}(Sb_4Se_9)^{6-}$ fragment present in the crystal structure of $Ba_2Sb_2Se_5$. Each split Se position is two-coordinated. Sb: blue; Se: orange.

The crystal structure of $Ba_2Sb_2Se_5$ consists of two one-dimensional building blocks separated by additional Ba atoms, ${}_{\infty}^{1}(Sb_4Se_9)^{6-}$ and ${}_{\infty}^{1}(Ba_2Se)^{2+}$ (Figure 3, left). The former fragment consists of $SbSe_5$ square pyramids that share all square vertices. The ${}_{\infty}^{1}(Sb_4Se_9)^{6-}$ one-dimensional slab is built by condensing four pyramids in the direction perpendicular to the direction of slab propagation, the [001] direction, with two apical vertices up and two down (Figures 2 and 3). All Sb atoms are situated almost in a single plane with an ∠Sb-Sb-Sb angle of 170.4°. The Se atoms that are surrounded by four antimony atoms are disordered in the manner that is described above in Figures 1 and 2. Thus, each of these Se atoms is two-coordinated. Bonding Sb-Se distances in the crystal structure of $Ba_2Sb_2Se_5$ fall in the range of 2.52-2.79 Å, which is comparable to distances found in $Ba_4Sb_4Se_{11}$,[14] $BaSb_2Se_4$,[15] and $Ba_3Sb_2Se_7$.[16] In the flat ${}_{\infty}^{1}(Ba_2Se)^{2+}$ fragment each Se atom is surrounded by a square of Ba atoms. The Ba-Se distances in this

Journal of Materials Chemistry C Accepted Manuscript

fragment (3.21 Å) are the shortest Ba-Se distances in the whole crystal structure, all other Ba-Se distances are at least 0.1 Å longer. Assuming +2, +3, and –2 formal oxidation states for Ba, Sb, and Se, respectively, total electroneutrality is achieved: $(Ba^{2+})_2(Sb^{3+})_2(Se^{2-})_5$. $Ba_2Sb_2Se_5$ is expected to exhibit semiconducting properties, which was further proved by resistivity and optical spectroscopy measurements.

$Ba_6Sb_7Se_{16.11}$ exhibits a more complex crystal structure with severe disorder in the Se sublattice and a *b* unit cell parameter larger than 62 Å (Figure 3 right and Table 1). The crystal structure of $Ba_6Sb_7Se_{16.11}$ consists of four main structural units and additional Ba atoms: ${}_{\infty}^{2}(Sb_4Se_6)^0$, ${}_{\infty}^{1}(Sb_3Se_7)^{5-}$, ${}_{\infty}^{1}(SbSe_3)^{3-}$, and ${}_{\infty}^{1}(Ba_2Se)^{2+}$. The latter fragment, with Ba-Se distances of 3.22 Å, is very similar to the fragment present in the crystal structure of $Ba_2Sb_2Se_5$. The one dimensional ${}_{\infty}^{1}(Sb_3Se_7)^{5-}$ slab is composed of only three $SbSe_5$ tetragonal pyramids in a manner similar to the one-dimensional Sb-Se slab present in the crystal structure of $Ba_2Sb_2Se_5$. However, the ${}_{\infty}^{1}(Sb_3Se_7)^{5-}$ slab is not flat but significantly bent with an ∠Sb-Sb-Sb angle of 142.6°. The ${}_{\infty}^{1}(SbSe_3)^{3-}$ one dimensional fragment is a tetrahedral chain composed of $SbSe_4$ tetrahedra sharing two vertices. Finally, large two dimensional, neutral ${}_{\infty}^{2}(Sb_4Se_6)^0$ layers are formed by condensing alternating $SbSe_5$ square pyramids and $SbSe_3$ pyramids connected to each other by sharing all vertices except the apical vertices of $SbSe_5$. Severe disorder is present in the Se sublattice (Table 2). Most of the Se positions surrounded by four antimony atoms are split in a manner similar to the crystal structure of $Ba_2Sb_2Se_5$, see Figures 1 and 2. Both of the Sb and Se atomic positions in the ${}_{\infty}^{1}(SbSe_3)^{3-}$ tetrahedral chains are split (Figure 3, bottom right). In addition, two Se positions, which are shared Se positions in the tetrahedral chains, are not fully occupied, *i.e.* the refined occupancies of the split positions are significantly smaller than 50%. This results in the non-integer composition of $Ba_6Sb_7Se_{16.11}$. Full occupancy, *viz.* 50%, of those two split Se positions, Se(17) and Se(18) in Table 2, would result in the composition $Ba_6Sb_7Se_{16.75}$, which is not electron balanced. Assuming +2, +3, and –2 formal oxidation states for Ba, Sb, and Se respectively, the electron-balanced composition is $(Ba^{2+})_6(Sb^{3+})_7(Se^{2-})_{16.5}$. Thus, $Ba_6Sb_7Se_{16.11}$ is expected to exhibit metallic properties with electrons as the main charge carriers since the experimental composition can be written as $(Ba^{2+})_6(Sb^{3+})_7(Se^{2-})_{16.1}(e^-)_{0.8}$. The presence of admixtures prevented us from characterizing the physical properties of $Ba_6Sb_7Se_{16.11}$.

Journal of Materials Chemistry C Accepted Manuscript

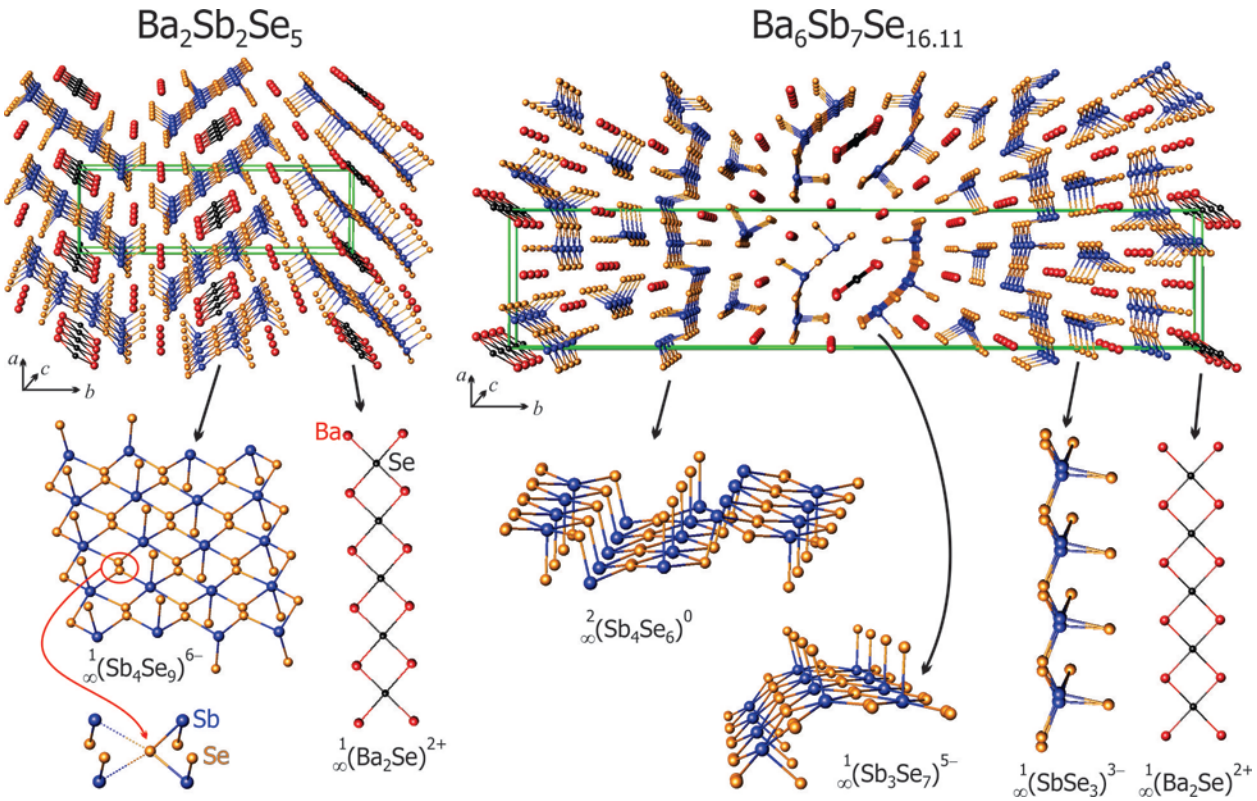

Figure 3. The crystal structure of (left) $Ba_2Sb_2Se_5$ and (right) $Ba_6Sb_7Se_{16.11}$. Top: general view; bottom: constituent fragments. Note that most of the Se sites are split and disordered. Fully ordered Se sites are only found in the $_\infty^1(Ba_2Se)^{2+}$ fragment and the apical Se position in the $_\infty^1(Sb_4Se_9)^{6-}$, $_\infty^2(Sb_4Se_6)^0$, and $_\infty^1(Sb_3Se_7)^{5-}$ fragments. Ba: red; Sb: blue; Se: orange and black.

SbQ_3 pyramidal and SbQ_5 square pyramidal units (Q = S, Se) are common fragments in the crystal structures of various AE-Sb-Q compounds (AE = alkaline-earth metal). Several such pyramids can be condensed together into either larger finite fragments or into one-dimensional chains. For example, in the crystal structure of $Sr_3Sb_4S_9$, the SbS_3 and SbS_5 pyramids form $_\infty^1(Sb_4S_9)^{6-}$ one-dimensional slabs,[17] which are similar to the one-dimensional Sb-Se fragments found in $Ba_2Sb_2Se_5$. In the crystal structure of $Ba_4Sb_4Se_{11}$ the $_\infty^1(SbSe_3)^{2-}$ chains are formed via the formation of the Se-Se bonds between the Sb_2Se_6 double tetrahedra.[14] The $_\infty^1(SbSe_2)^{1-}$ chains consisting of edge sharing $SbSe_3$ pyramids and $SbSe_5$ square pyramids are present in the crystal structure of $BaSb_2Se_4$.[15] The more complicated crystal structure of $SrSbSe_3$ can be

Journal of Materials Chemistry C Accepted Manuscript

described as a combination of one-dimensional $_\infty^1(Sb_4Se_9)^{6-}$ tubular columns together with isolated Se_3^{2-} anions.[18] The isolated SbQ_x, (x = 3, 4, 5) fragments are also observed in the crystal structures of $Ba_8Sb_6S_{17}$,[19] $Ca_2Sb_2S_5$,[20] and $Ba_3Sb_2Se_7$.[16] The larger isolated units are found in the crystal structures of $Sr_6Sb_6S_{17}$[21] and $Ba_8Sb_6S_{17}$,[19] in which the $[Sb_3S_8]^{7-}$ fragments composed of three corner-sharing SbS_3 trigonal pyramids are the main building blocks. Despite the similarity in elemental composition of $Ca_2Sb_2S_5$ and $Ba_2Sb_2Se_5$, the crystal structure of $Ca_2Sb_2S_5$ is different from the crystal structure of $Ba_2Sb_2Se_5$.[20] The crystal structure of $Ca_2Sb_2S_5$ (monoclinic, space group $P2_1/c$) is composed of isolated $(SbS_3)^{3-}$ pyramids and $(Sb_2S_4)^{2-}$ quadrangles separated by Ca^{2+} cations.

Physical Properties. Solid-state UV-visible spectroscopy was employed to determine the experimental bandgap of $Ba_2Sb_2Se_5$. Several samples were measured and two typical spectra are shown in Figure 4, top.

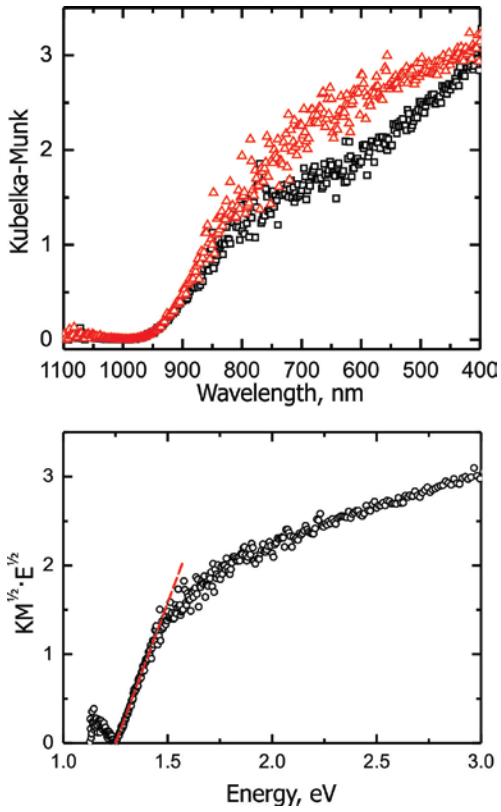

Figure 4. Top: Kubelka-Munk diffuse reflectance solid-state UV-visible spectra of $Ba_2Sb_2Se_5$. Two typical measurements are shown by red and black symbols. Bottom: Tauc plot for allowed indirect transitions.

Journal of Materials Chemistry C Accepted Manuscript

All measured samples exhibited absorption onsets at 970 nm. According to the calculated Tauc plots, $Ba_2Sb_2Se_5$ exhibits an indirect optical transition corresponding to a bandgap of 1.25(5) eV.

The resistivity of $Ba_2Sb_2Se_5$ decreases with increasing temperature from 280 – 400 K, indicating thermally activated behavior that is typical for semiconductors (Figure 5). At temperatures below 280 K the resistivity was too high to be measured using the PPMS. Using the equation $\ln(1/\rho) = \ln(1/\rho_0) - E_a/2kT$, the linear dependence of $\ln(1/\rho)$ *vs.* 1/T was fit to give an activation energy of 0.9(1) eV, which is in good agreement with the indirect band gap of 1.25(5) eV determined by UV-visible spectroscopy measurements (Figure 5 inset). The resistivity of $Ba_2Sb_2Se_5$ at 400 K is 70 Ω·m, which is too high for practical thermoelectric applications.

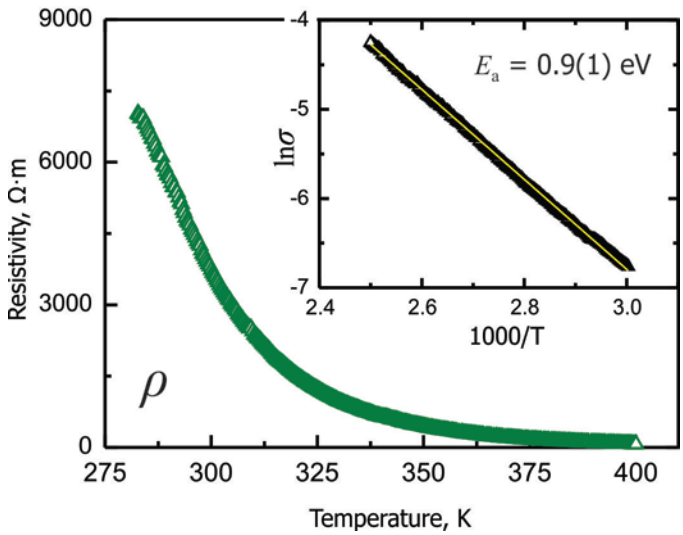

Figure 5. Temperature dependence of the resistivity of $Ba_2Sb_2Se_5$. Inset: linear fit (yellow line) of the $\ln(1/\rho)$ *vs.* 1/T dependence (black triangles).

Journal of Materials Chemistry C Accepted Manuscript

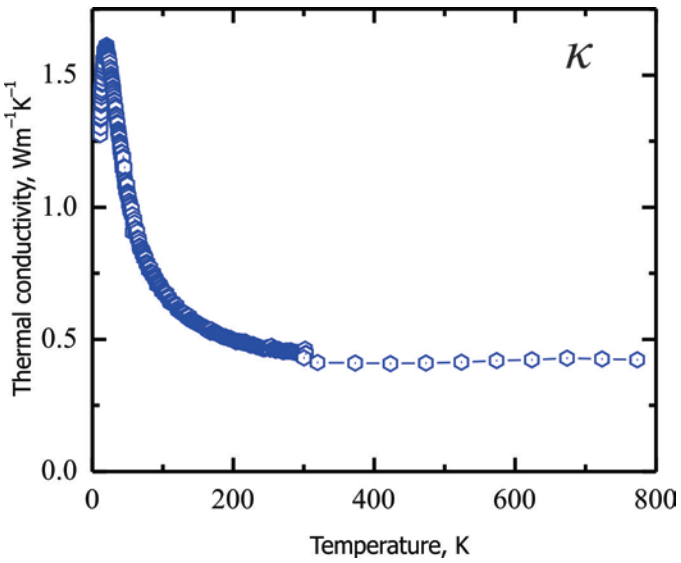

Figure 6. Temperature dependence of the thermal conductivity of $Ba_2Sb_2Se_5$.

The thermal conductivity was measured on the polycrystalline $Ba_2Sb_2Se_5$ sample compacted using spark plasma sintering (SPS). The geometrical density of the pellet was 95% of the theoretical value. Powder X-ray diffraction of the sample prior to and after SPS treatment indicates that no decomposition of the sample occurs as a result of the sintering (Figure S1). Powder X-ray diffraction of the SPS pellet indicates that some texturing occurs due to sintering since certain redistribution of the intensities was observed for in-plane and out-of-plane powder diffraction patterns (Figure S4). Preferred orientation of the crystallites is an expected effect for strongly anisotropic compound.

The thermal conductivity of $Ba_2Sb_2Se_5$ is shown in Figure 6. The thermal conductivity first increases from 2 – 20 K and reaches a maximum (1.6 $Wm^{-1}K^{-1}$), which is typical for crystalline solids. As temperature increases, the thermal conductivity decreases down to a value of 0.45 $Wm^{-1}K^{-1}$ at 300 K. At higher temperatures the thermal conductivity values remain in the range of 0.41-0.45 $Wm^{-1}K^{-1}$. At room temperature the estimated electronic contribution using the Wiedemann-Franz law is negligible, less than 1% of the total thermal conductivity.[22] The extremely low lattice thermal conductivity stems from the one dimensional crystal structure with a large primitive unit cell containing 36 heavy atoms as well as from the substantial structural disorder in the Se sublattice. The presence of such disorder prevents us from calculating the electronic structure of this compound.

Journal of Materials Chemistry C Accepted Manuscript

Understanding how low lattice thermal conductivity is achieved in solids is important for designing efficient thermoelectric materials. The low thermal conductivity of $Ba_2Sb_2Se_5$ is comparable to or smaller than that of some of the state-of-art thermoelectric materials, such as $Yb_{14}MnSb_{11}$ (0.7 $Wm^{-1}K^{-1}$ at 300 K),[23] *n*-type $Ba_8Ga_{16}Sn_{30}$ (0.4 $Wm^{-1}K^{-1}$ at 300 K),[24] $Bi_{0.5}Sb_{1.5}Te_3$ (0.7 $Wm^{-1}K^{-1}$ at 300 K),[25] the [010] direction of a SnSe single crystal (0.7 $Wm^{-1}K^{-1}$ at 300 K),[26] and Ca_3AlSb_3 (1.3 $Wm^{-1}K^{-1}$ at 300 K).[27] Extremely low lattice thermal conductivity can be achieved in compounds with i) complex crystal structures with a large number of heavy atoms in the primitive unit cell (*e.g.*, $Ba_8Au_{16}P_{30}$,[28] $Gd_{117}Co_{56}Sn_{112}$,[29] and Ag_9TlTe_5[30] all exhibit lattice thermal conductivities below 0.5 $Wm^{-1}K^{-1}$ at 300 K) and ii) simple crystal structures where significant structural inhomogenieties due to elemental segregation and nanostructuring of domains of different compositions are present: doped-Pb*Q* (*Q* = S, Se, and/or Te),[31-38] LAST materials,[4] $LiPbSb_3S_6$,[39] and $Li_{1-x}Sn_{2+x}As_2$.[40] For these materials the lattice thermal conductivities vary between 0.5-2 $Wm^{-1}K^{-1}$ at 300 K. The low thermal conductivity in $Ba_2Sb_2Se_5$ is due to a combination of both reasons: a complex crystal structure and the presence of disorder at the atomic level. A similar extremely low value of the total thermal conductivity, 0.3 $Wm^{-1}K^{-1}$ at 300 K, was reported for $Ag_{10}Te_4Br_3$, which exhibited complex structural disorder in the Te and Ag sublattices.[41]

$Ba_2Sb_2Se_5$ exhibits a Seebeck thermopower of –620 μV/K at 300 K (Figure S3), which is expected for the highly resistive compound with a low carrier concentration. The negative sign of the Seebeck coefficient indicates that electrons are the main charge carriers. Due to the high resistivity, the figure of merit of $Ba_2Sb_2Se_5$ is only $ZT = 3.7\cdot10^{-6}$ at 300 K. The ultra-low lattice thermal conductivity and high Seebeck thermopower are attractive properties for thermoelectric materials. To achieve a higher thermoelectric figure-of-merit, the resistivity should be reduced by several orders of magnitude. Doping more electrons into system, *viz.* La^{3+} for Ba^{2+} substitution, may result in the desired reduction in resistivity, though doping may also reduce the Seebeck thermopower. Investigations of substituted systems are currently underway.

Experimental section

Synthesis. All preparation and handling of samples were performed in an argon-filled glovebox with the O_2 level below 1 ppm. All starting materials were commercial grade and used as

Journal of Materials Chemistry C Accepted Manuscript

received: Ba (Sigma Aldrich, 99.9%), Sb (Alfa Aesar, shots 99.9999%), and Se (Alfa Aesar, powder 99.999%).

The title compounds were synthesized from pure elements via conventional high-temperature solid-state reactions. To synthesize $Ba_2Sb_2Se_5$ and $Ba_6Sb_7Se_{16.11}$, the reactants were loaded in stoichiometric ratios, 2:2:5 and 6:7:16.11, respectively, into carbonized silica ampoules, evacuated, and flame-sealed. The ampoules were heated in muffle furnaces to 773 K at a rate of 50 K/h, and then annealed at this temperature for 24 h. Then the ampoules were heated up to 1073 K over 10 h and annealed at this temperature for 168 h. Finally the ampoules were cooled down to 773 K over 24 h and annealed for 96 h at this temperature, and afterwards the furnace was turned off. The $Ba_2Sb_2Se_5$ and $Ba_6Sb_7Se_{16.11}$ products were black, polycrystalline air-sensitive powders. According to powder X-ray diffraction, the $Ba_2Sb_2Se_5$ sample was a single phase (Figure S1), while the yield of $Ba_6Sb_7Se_{16.11}$ was only ~70% and significant amounts of $Ba_4Sb_4Se_{11}$ [14] were present. All our attempts to synthesize single-phase samples of $Ba_6Sb_7Se_{16.11}$ by varying the temperature profile were unsuccessful.

X-ray powder diffraction and elemental analysis. The samples were characterized by powder X-ray diffraction (PXRD) using a Rigaku Miniflex 600 diffractometer employing Cu-K_α radiation. Elemental analysis of selected single crystals was carried out on a Hitachi S4100T scanning electron microscope (SEM) with energy-dispersive X-ray (EDX) microanalysis (Oxford INCA Energy). The analyses confirmed the presence of only Ba, Sb, and Se in the samples (Tables S1 and S2).

Single crystal X-ray diffraction. Data were collected at 90 K using a Bruker AXS SMART diffractometer with an APEX-II CCD detector with Mo-K_α radiation. The data sets were recorded as ω-scans with a 0.4° step width and integrated with the Bruker SAINT software package.[42] Multi-scan absorption corrections were applied.[42] The solution and refinement of the crystal structures were carried out using the SHELX suite of programs.[43] The final refinements were performed using anisotropic atomic displacement parameters for all atoms. A summary of pertinent information relating to the unit cell parameters, data collection, and refinements is provided in Table 1 and the atomic parameters and interatomic distances are provided in Tables 2 and 3. Further details of the crystal structure determination may be obtained

Journal of Materials Chemistry C Accepted Manuscript

from Fachinformations-zentrum Karlsruhe, D-76344 Eggenstein-Leopoldshafen, Germany, by quoting the depository numbers CSD-429623 ($Ba_2Sb_2Se_5$) and CSD-429624 ($Ba_6Sb_7Se_{16.11}$).

Sample densification. Polycrystalline samples of $Ba_2Sb_2Se_5$ were carefully ground into a fine powder, loaded into the graphite SPS die in the glovebox, and then sintered at 873 K through spark plasma sintering (Dr. Sinter Lab Jr. SPS-211Lx, Sumitomo Coal Mining Co, Ltd.) for 10 min with a uniaxial pressure of 80 MPa and under dynamic vacuum to form a pellet with dimensions of ~ ∅ 12.7 mm × 2 mm. The geometrical density of the pellet was 95% of the theoretical value. Graphite and any possible surface contaminations were removed by polishing the pellet in the glovebox. The sample purity after SPS was checked by PXRD and no sample decomposition was detected (Figure S1).

Diffuse reflectance spectroscopy. UV-visible diffuse reflectance spectra of $Ba_2Sb_2Se_5$ were recorded using a Thermo Scientific Evolution 220 Spectrometer equipped with an integrating sphere. The reflectance data, R, were converted using the Kubelka-Munk function $f(R) = (1 - R)^2(2R)^{-1}$.

Physical properties. The electrical resistivity was measured by a standard four-point alternating-current technique to exclude the resistance of the leads using the commercial multipurpose Physical Properties Measurement System (PPMS, Quantum Design). The Seebeck thermopower and thermal conductivity in the 2 – 300 K temperature range were measured using the Thermal Transport Option (PPMS). High-temperature (300 – 800 K) thermal diffusivity data for $Ba_2Sb_2Se_5$ were directly measured using a Netzsch LFA-457 instrument (Figure S2). The heat capacity of $Ba_2Sb_2Se_5$ was approximated using the simultaneously measured standard Pyroceram 9606 (Figure S2). The thermal conductivity was calculated using the equation $\kappa = D\rho C_p$, where D is the thermal diffusivity, ρ is the room temperature density, and C_p is the calculated heat capacity.

Journal of Materials Chemistry C Accepted Manuscript

Table 1. Selected single crystal data collection and structure refinement parameters for $Ba_2Sb_2Se_5$ and $Ba_6Sb_7Se_{16.11}$.

Composition	$Ba_2Sb_2Se_5$	$Ba_6Sb_7Se_{16.11(2)}$
Formula weight	912.98 g/mol	2948.73 g/mol
Temperature	90(2) K	
Radiation, wavelength	Mo-Kα, 0.71073 Å	
Crystal system	orthorhombic	
Space group	*Pbam* (No. 55)	*Pnnm* (No. 58)
Unit cell dimensions	a = 8.403(2) Å	a = 12.469(2) Å
	b= 27.567(5) Å	b = 62.421(7) Å
	c = 4.6422(8) Å	c = 4.6305(5) Å
Unit cell volume	1075.4(3) Å^3	3604.1(7) Å^3
Z	4	
Density (*calc.*)	5.64 g/cm^3	5.43 g/cm^3
Absorption coefficient	29.05 mm^{-1}	27.86 mm^{-1}
Data/parameters	1139/62	3330/235
Goodness-of-Fit	1.06	1.07
Final R indices [a] [$I > 2\sigma(I)$]	R_1 = 0.031	R_1 = 0.036
	wR_2 = 0.061	wR_2 = 0.061
Final R indices [a] [all data]	R_1 = 0.042	R_1 = 0.051
	wR_2 = 0.066	wR_2 = 0.066

$R_1 = \sum||F_o| - |F_c||/\sum|F_o|$; $wR_2 = [\sum[w(F_o^2 - F_c^2)^2]/\sum[w(F_o^2)^2]]^{1/2}$, and $w = 1/[\sigma^2F_o^2 + (A\cdot P)^2 + B\cdot P]$, $P = (F_o^2 + 2F_c^2)/3$; A and B are weight coefficients.

Journal of Materials Chemistry C Accepted Manuscript

Table 2. Refined atomic coordinates and equivalent displacement parameters for $Ba_2Sb_2Se_5$ and $Ba_6Sb_7Se_{16.11}$.

Atom	Wyckoff	*x/a*	*y/b*	*z/c*	*Occupancy*	U_{eq} (Å^2)
				$Ba_2Sb_2Se_5$		
Ba1	4*h*	0.00348(9)	0.29850(3)	0.5	1	0.0082(2)
Ba2	4*h*	0.34019(9)	0.43613(3)	0.5	1	0.0084(2)
Sb1	4*g*	0.0581(1)	0.15828(4)	0	1	0.0118(2)
Sb2	4*g*	0.3701(1)	0.05856(3)	0	1	0.0089(2)
Se1	8*i*	0.2267(2)	0.10507(7)	0.4095(4)	0.5	0.0082(4)
Se2	4*h*	0.3935(2)	0.31734(6)	0.5	1	0.0329(5)
Se3	4*g*	0.1108(2)	0.38306(5)	0	1	0.0116(3)
Se4	4*g*	0.2272(2)	0.23383(5)	0	1	0.0131(3)
Se5	4*f*	0	0.5	0.3949(6)	0.5	0.0073(5)
Se6	2*a*	0	0	0	1	0.0256(6)
				$Ba_6Sb_7Se_{16.11(2)}$		
Ba1	4*g*	0.03326(7)	0.46352(2)	0	1	0.0105(2)
Ba21	4*g*	0.0502(1)	0.71450(3)	0	0.967(4)	0.0273(4)
Ba22	4*g*	0.049(3)	0.7281(9)	0	0.033(4)	0.0273(4)
Ba3	4*g*	0.09204(8)	0.35743(2)	0	1	0.0153(2)
Ba4	4*g*	0.19189(7)	0.59286(2)	0	1	0.0110(2)
Ba5	4*g*	0.39298(7)	0.47126(2)	0	1	0.0118(2)
Ba6	4*g*	0.48048(8)	0.36436(2)	0	1	0.0173(2)
Sb1	8*h*	0.3276(1)	0.15850(2)	0.0544(7)	0.5	0.0219(9)
Sb2	4*g*	0.01919(9)	0.07439(2)	0	1	0.0160(3)
Sb3	4*g*	0.71522(8)	0.08470(2)	0	1	0.0119(2)
Sb41	4*g*	0.2558(2)	0.26079(4)	0	0.556(10)	0.022(2)
Sb42	4*g*	0.2541(4)	0.26097(7)	-0.1120(2)	0.222(5)	0.022(2)
Sb51	4*g*	0.2277(1)	0.02963(2)	0	0.768(2)	0.0125(3)
Sb52	4*g*	0.2894(4)	0.02163(8)	0	0.232(2)	0.0125(3)
Sb61	8*h*	0.3151(2)	0.32138(4)	0.4411(6)	0.484(3)	0.024(1)
Sb62	4*g*	0.339(4)	0.3314(1)	0.5	0.033(6)	0.024(1)

Journal of Materials Chemistry C Accepted Manuscript

Sb71	4*g*	0.5688(1)	0.28947(2)	0	0.901(3)	0.0179(4)
Sb72	4*g*	0.5570(10)	0.2759(3)	0	0.099(3)	0.0179(4)
Se1	8*h*	0.0859(2)	0.41091(3)	0.0562(6)	0.5	0.0089(9)
Se2	8*h*	0.1244(2)	0.05441(3)	0.4150(4)	0.5	0.0118(6)
Se3	8*h*	0.3088(2)	0.00753(3)	0.4226(4)	0.5	0.0142(7)
Se4	8*h*	0.3782(2)	0.41421(3)	0.0929(4)	0.5	0.0116(5)
Se5	8*h*	0.4081(2)	0.26645(4)	0.4404(8)	0.5	0.030(1)
Se6	4g	0.0190(1)	0.17356(3)	0	1	0.0225(4)
Se7	4*g*	0.1258(1)	0.10941(3)	0	1	0.0125(4)
Se8	4*g*	0.2589(1)	0.21940(3)	0	1	0.0240(4)
Se9	4*g*	0.3839(1)	0.05842(2)	0	1	0.0113(3)
Se10	4*g*	0.4260(1)	0.12261(3)	0	1	0.0182(4)
Se11	4*g*	0.5070(1)	0.17846(3)	0	1	0.0196(4)
Se12	4*g*	0.1051(2)	0.26255(4)	-0.4462(1)	0.5	0.026(1)
Se13	4*g*	0.7190(1)	0.04352(2)	0	1	0.0106(3)
Se14	4*g*	0.7823(1)	0.13721(3)	0	1	0.0185(4)
Se15	2*a*	0	0	0	1	0.0223(6)
Se16	8*h*	0.0249(5)	0.5015(2)	0.5	0.25	0.014(2)
Se17	8*h*	0.2584(3)	0.31253(5)	0.0655(8)	0.353(5)	0.029(2)
Se18	8*h*	0.2497(3)	0.16373(6)	0.4354(8)	0.330(4)	0.022(2)

[a] U_{eq} is defined as one third of the trace of the orthogonalized U^{ij} tensor.

Journal of Materials Chemistry C Accepted Manuscript

Table 3. Selected interatomic distances (Å) in $Ba_2Sb_2Se_5$ and $Ba_6Sb_7Se_{16.11}$.

Atom pairs	Distances (Å)	Atom pairs	Distances (Å)
		$Ba_2Sb_2Se_5$	
Ba1 – Se1× 2	3.557(2)	Ba2 – Se1× 2	3.466(2)
Se2	3.319(2)	Se2	3.305(2)
Se2	3.324(2)	Se3× 2	3.353(1)
Se3	3.411(1)	Se5× 2	3.393(1)
Se3	3.411(1)	Sb1– Se1× 2	2.788(2)
Se4× 2	3.402(1)	Se2× 2	2.784(1)
Se4	3.478(1)	Se4	2.521(2)
Se4	3.479(13)	Sb2– Se1× 2	2.590(2)
		Se3	2.585(2)
		Se5× 2	2.676(2)
		$Ba_6Sb_7Se_{16.11}$	
Ba1– Se1× 2	3.359(2)	Sb2– Se2× 2	2.640(2)
Se3× 2	3.351(2)	Se4× 2	2.674(2)
Se9× 2	3.272(2)	Se7	2.558(2)
Se13× 2	3.304(2)	Sb3– Se1× 2	2.626(3)
Se16× 2	3.265(1)	Se4× 2	2.772(2)
Se16× 2	3.314(1)	Se13	2.571(2)
Ba21/Ba22– Se5× 2	3.296(3)	Sb41– Se5× 2	2.809(4)
Se8× 2	3.335(2)	Se8	2.584(3)
S11× 2	3.306(2)	Se12× 2	2.795(4)
S12× 2	3.173(4)	Sb42– Se5	2.452(7)
Ba3 – Se1× 2	3.350(2)	Se5	2.821(7)
Se10× 2	3.347(1)	Se8	2.654(5)
Se11× 2	3.392(1)	Se12	2.397(7)
Se14× 2	3.332(1)	Se12	2.739(7)

Journal of Materials Chemistry C Accepted Manuscript

Ba4–	Se2× 2	3.341(2)	Sb51–	Se2× 2	2.783(2)
	Se7× 2	3.405(1)		Se3× 2	2.599(2)
	Se9× 2	3.297(1)		Se9	2.650(2)
	Se10× 2	3.312(1)	Sb52–	Se3× 2	2.825(3)
Ba5–	Se2× 2	3.324(2)		Se9	2.581(5)
	Se3× 2	3.404(2)		Se16	2.635(9)
	Se13× 2	3.304(1)	Sb61–	Se6	2.578(3)
	Se15× 2	3.219(1)		Se14	2.631(3)
Ba6–	Se4× 2	3.391(2)		Se17	1.956(5)
	Se6× 2	3.346(1)		Se17	2.454(4)
	Se7× 2	3.365(1)		Se17	2.511(5)
	Se14× 2	3.388(1)	Sb62–	Se6	2.27(5)
Sb1 –	Se10	2.567(2)		Se17× 2	2.54(4)
	Se11	2.573(2)	Sb71/Sb72–	Se5× 2	2.82 (1)
	Se18	2.488(4)		Se12	2.48(2)
	Se18	2.575(4)			
	Se18	2.040(5)			

Conclusions

Two new barium antimony selenides, $Ba_2Sb_2Se_5$ and $Ba_7Sb_6Se_{16}$, have been synthesized. Each compound crystallizes in its own new structure type, featuring the presence of disordered one- and two-dimensional Sb-Se fragments separated by Ba cations and one-dimensional Ba_2Se chains. $Ba_2Sb_2Se_5$ exhibits semiconducting properties with an indirect bandgap close to 1 eV as revealed by resistivity measurements and optical absorption spectroscopy. The lattice thermal conductivity of $Ba_2Sb_2Se_5$ is lower than 0.5 $Wm^{-1}K^{-1}$ in the 200 – 800 K temperature range. To achieve high thermoelectric efficiency, heavy doping of $Ba_2Sb_2Se_5$ is required to reduce the currently high electrical resistivity.

Journal of Materials Chemistry C Accepted Manuscript

Acknowledgments

We thank Prof. S. M. Kauzlarich for access to the LFA and SPS and Prof F. Osterloh for access to the UV-visible diffuse reflectance spectrometer. K. L. acknowledges the GAANN fellowship. This research is supported by the U.S. Department of Energy, Office of Basic Energy Sciences, Division of Materials Sciences and Engineering under Award DE-SC0008931.

References

[1] I. Chung, M. G. Kanatzidis, *Chem. Mater.*, 2014, **26**, 849-869.

[2] W. Y. Hao, D. J. Mei, W. L. Yin, K. Feng, J.Y. Yao, Y. C. Wu, *J. Solid State Chem.*, 2013, **198**, 81-86.

[3] D.-Y. Chung, T. Hogan, P. Brazis, M. Rocci-Lane, C. Kannewurf, M. Bastea, C. Uher, M. G. Kanatzidis, *Science*, 2000, **287**, 1024-1027.

[4] K. F. Hsu, S. Loo, F. Guo, W. Chen, J. S. Dyck, C. Uher, T. Hogan, E. K. Polychroniadis, M. G. Kanatzidis, *Science*, 2004, **303**, 818-821.

[5] Y. S. Zh, V. Ozoliņš, D. Morelli, C. Wolverton, *Chem. Mater.*, 2014, **26**, 3427-3435.

[6] K. Tyagi, B. Gahtori, S. Bathula, A. K. Srivastava, A. K. Shukla, S. Aulucka, A. Dhar, *J. Mater. Chem. A.*, 2014, **2**, 15829-15835.

[7] W. J. Qiu, L. L. Xi, P. Wei, X. Z. Ke, J. H. Yang, W. Q. Zh, *Proc. Natl. Acad. Sci. U.S.A.*, 2014, **111**, 15031-15035.

[8] T-R. Wei, C-F. Wu, W. Sun, Y. Pan, J-F. Li, *RSC Adv.*, 2015, **5**, 42848-42854.

[9] K. Tyagi, B. Gahtori, S. Bathula, V. Toutam, S. Sharma, N. K.Singh, A. Dhar, *Appl. Phys. Lett.*, 2014, **105**, 261902.

[10] D. Do, V. Ozolins, S. D. Mahanti, M.-S. Lee, Y.-S. Zhang, C. Wolverton, *J. Phys.: Condens. Matter*, 2012, **24**, 415502.

[11] Y.Y. Li, D. Li, X. Y. Qin, X.H. Yang, Y. F. Liu, J. Zhang, Y.C. Dou, C. J. Song, H. X. Xin, *J. Mater. Chem. C*, 2015, **DOI**: 10.1039/C5TC01318F.

Journal of Materials Chemistry C Accepted Manuscript

[12] H. Djieutedjeu, P. F. P. Poudeu, N. J. Takas, J. P. A. Makongo, A. Rotaru, K. G. S. Ranmohotti, , C. J. Anglin, L. Spinu, J. B. Wiley, *Angew. Chem. Int. Ed.*, 2010, **49**, 9977-9981.

[13] K. G. S. Ranmohotti, H. Djieutedjeu , J. Lopez , A. Page , N. Haldolaarachchige, H. Chi , P. Sahoo, C. Uher , D. Young , P. F. P. Poudeu, *J. Am. Chem. Soc.*, 2015, **137**, 691-698.

[14] G. Cordier, R. Cook, H. Schaefer, *Angew. Chem.*, 1980, **92**, 310.

[15] G. Cordier, H. Schaefer, *Z. Naturforsch. B.*, 1979, **34**, 1053-1056.

[16] J. Wang, K. Lee, K. Kovnir. *Z. Anorg. Allg. Chem.*, 2015, **641(6)**, 1087-1092.

[17] G. Cordier,C. Schwidetzky, H. Schaefer, *Rev. Chim. Miner.*, 1982, **19**, 179-186.

[18] R. Cook, H. Schaefer, *Stud. Inorg. Chem.*, 1983, **3**, 757-760.

[19] W. Doerrscheidt, H. Schaefer, *Z.Naturforsch.Pt. B.*, 1981, **36**, 410-414.

[20] G. Cordier, H. Schaefer, *Rev. Chim. Miner.*, 1981, **18**, 218-223.

[21] K.-S. Choi, M. G. Kanatzidis, *Inorg. Chem.*, 2000, **39**, 5655-5662.

[22] H.-S. Kim, Z. M. Gibbs, Y. Tang, H. Wang, G. J. Snyder, *APL Mater*, 2015, **3**, 041506.

[23] S. R. Brown, S. M. Kauzlarich, F. Gascoin, G. J. Snyder, *Chem. Mater*., 2006, **18**, 1873-1877.

[24] Y. Saiga, K. Suekuni, B. Du, T. Takabatake, *Solid. State. Commun*., 2012,**152**, 1902-1905.

[25] B. Poudel, Q. Hao, Y. Ma, Y. Lan, A. Minnich, B. Yu, X. Yan, D. Wang, A. Muto, D. Vashaee, X. Chen, J. Liu, M. S. Dresselhaus, G. Chen, Z. F. Ren, *Science*, 2008 , *320*, 634-638.

[26] L-D. Zhao, S.-H. Lo, Y. Zhang, H. Sun, G.J. Tan, C. Uher, C. Wolverton, V. P. Dravid, M. G. Kanatzidis, *Nature*, 2014, **508**,373-377.

[27] (a) A. Zevalkink, E. S. Toberer, W. G. Zeier, E. Flage-Larsen, G. J. Snyder, *Energy Environ. Sci*., 2011, **4**, 510-518. (b) W. G. Zeier, A. Zevalkink, E. Schechtel, W. Tremel, G. J. Snyder, *J. Mater. Chem*., 2012, **22**, 9826-9830.

[28] J. Fulmer, O. I. Lebedev, V.V. Roddatis, D. Kaseman, S. Sen, J. Dolyniuk, K. Lee, A.V. Olenev, K. Kovnir, *J. Am. Chem. Soc.*, 2013**, 135**, 12313-12323.

Journal of Materials Chemistry C Accepted Manuscript

[29] D. C. Schmitt, N. Haldolaarachchige , Y. Xiong , D. P. Young , R. Jin , J. Y. Chan, *J. Am. Chem. Soc.*, 2012, **134** ,5965–5973.

[30] K. Kurosaki, A. Kosuga, H. Muta, M. Uno, S. Yamanaka, *Appl. Phys. Lett.*, 2005, **87**, 061919.

[31] J. P. Heremans, V. Jovovic, E. S. Toberer, A. Saramat, K. Kurosaki, A. Charoenphakdee, S. Yamanaka, G. J. Snyder, *Science*, 2008 , **321**, 554-557.

[32] Y. Z. Pei, X. Y. Shi, A. LaLonde, H. Wang, L. D. Chen, G. J. Snyder, *Nature*, 2011 , **473**, 66-69.

[33] Y. Z. Pei, J. Lensch-Falk, E. S. Toberer, D. L. Medlin, G. J. Snyder, *Adv. Funct. Mater*., 2011 , **21**, 241-249.

[34] P. F. P. Poudeu, J. D'Angelo, A. D. Downey, J. L. Short, T. P. Hogan, M. G. Kanatzidis, *Angew. Chem., Int. Ed.*, 2006, **45**, 3835-3839.

[35] J. Androulakis, C. H., Lin, H. J. Kong, C. Uher, C. I. Wu , T. Hogan, B. A. Cook, T. Caillat, K. M. Paraskevopoulos, M. G. Kanatzidis, *J. Am. Chem. Soc.*,2007, **129** ,9780-9788.

[36] K. Biswas, J. He, Q. Zhang, G. Wang, C. Uher, V. P. Dravid, M.G. Kanatzidis, *Nat. Chem.* 2011, **3**, 160-166.

[37] D. M. Rowe, CRC Handbook of Thermoelectrics. CRC, Boca Raton, 1995.

[38] J. Androulakis, I. Todorov, D.-Y. Chung, S. Ballikaya, G. Y. Wang, C. Uher, M. G. Kanatzidis, *Phys. Rev. B.*, 2010, **82**, 115209.

[39] E. C. Agha, C. D. Malliakas, J. Im, H. Jin , L.-D. Zhao, A. J. Freeman, M. G. Kanatzidis, *Inorg. Chem.*, 2014, **53**, 673-675.

[40] K. Lee, D. Kaseman, S. Sen, I. Hung, Z. Gan, B. Gerke, R. Pöttgen, M. Feygenson, J. Neuefeind, O. I. Lebedev, K. Kovnir, *J. Am. Chem. Soc.*, 2015, **137**, 3622-3630.

[41] T. Nilges, S. Lange, M. Bawohl, J.M. Deckwart, M. Janssen, H.-D. Wiemhöfer, R. Decourt, B. Chevalier, J. Vannahme, H. Eckert, R. Weihrich, *Nature. Mater.* 2009, **8**, 101-108.

[42] Bruker APEX2; Bruker AXS Inc.: Madison, WI, 2005.

[43] Sheldrick, G.M. *Acta Crystallogr. Sect. A.* 2008, **A64**, 112-122.

Journal of Materials Chemistry C Accepted Manuscript